Rabi-Bloch oscillations in spatially distributed systems: Temporal dynamics and frequency spectra

Ilay Levie,* Raphael Kastner, and Gregory Slepyan†
School of Electrical Engineering, Tel Aviv University, Tel Aviv 69978, Israel
(Received 17 April 2017; published 23 October 2017)

We consider one-dimensional chains of two-level quantum systems coupled via tunneling. The chain is driven by the superposition of dc and ac fields in the strong coupling regime. Based on the fundamental principles of electrodynamics and quantum theory, we have developed a generalized model of quantum dynamics for such interactions, free of rotating-wave approximation. The system of equations of motion was studied numerically. We analyzed the dynamics and spectra of the inversion density, dipole current density, and tunneling current density. In the case of resonant interaction with the ac component, the particle dynamics exhibits itself in the oscillatory regime, which may be interpreted as a combination of Rabi and Bloch oscillations with their strong mutual influence. Such scenario for an obliquely incident ac field dramatically differs from the individual picture of both types of oscillations due to the interactions. This effect is counterintuitive because of the existence of markedly different frequency ranges for such two types of oscillations. These dynamics manifest themselves in multiline spectra in different combinations of Rabi and Bloch frequencies. The effect is promising as a framework of a new type of spectroscopy in nanoelectronics and electrical control of nanodevices.

DOI: 10.1103/PhysRevA.96.043854

I. INTRODUCTION

Periodic low-dimensional lattices have been investigated as platforms for many quantum phenomena for almost a century. They first appeared in the literature in the context of models for ferromagnetism in statistical mechanics (the Ising chain [1] and the Heisenberg spin chain [2]), and later in the simple model of interacting particles in a lattice describing the transition between conducting and insulating systems (the Hubbard chain [3]). Subsequent developments addressed various domains of periodicity, i.e., lattices in physical space, in time, in momentum space, involving spatial-periodic forces, time-periodic forces, etc., and certain combinations thereof. These developments covered actual embodiments of lattice elements, be it an atom, an ion, a molecule, or a quantum dot, and the mechanisms of their chain-formed interaction such as dipole-dipole interactions, exchange interactions, Coulomb interactions, and tunneling effects. More recently, rapid progress in atomic optics and nanotechnologies has facilitated experimental investigations of a number of physical systems, e.g., semiconducting and graphene superlattices [4,5], Bose-Einstein condensate trapped in an optical lattice [6], trapped ions chain [7,8], cooled atomic array in the cavity [9], the array of Josephson contacts [10], crystalline arrays of quantum dots connected by conducting chains of linker atoms or interacted via another physical mechanisms [11–15], conjugated polymer chains [16], and a lattice of p-wave superconductor in one dimension (the Kitaev chain) [17]. All of these systems are characterized by certain qualitative features that define the properties of their energy spectra and transport properties. These properties are important when one considers interactions with classical and quantum electromagnetic fields in the microwave, terahertz, and visible frequency ranges. Low-dimensional nanostructures are differentiated from traditional bulk materials by these properties, thereby enabling potential applications in nanoelectronics and nanophotonics, quantum informatics, and quantum computing [18].

Recent theoretical progress has been made in the areas of array types and interelement interactions. Examples include mechanisms of dissipative interelement interactions [19] and noisy coupling [20], which cause rather surprising thermodynamic behaviors of the arrays, also verified experimentally [21]. Scully and his team [22] developed the concept of the superradiant lattice, which corresponds to a collection of three-level atoms in timed Dicke states. The lattice structure is based on electromagnetically induced transparency. It can be potentially extended to three dimensions or more, with new physics waiting to be analyzed.

One phenomenon that forms the basis for the present work is the Rabi wave [23–28]. These waves have been identified as the outcome of strong coupling of light with spatially distributed chains of two-level fermionic systems. This coupling brings about spatial motion of Rabi oscillations (ROs) in the form of quantum transition waves that are the Rabi waves. Here, light plays the role of refractive medium for the wave propagation. Among the many promising applications of Rabi waves, one may note, e.g., the electrically tunable, highly directive, optical nanoantennas [23,25,29,30].

Rabi waves are combined in this work with the unrelated phenomenon of Bloch oscillations (BOs) of a single particle in a periodic potential under the influence of a static force. Initially, the question of how electrons would behave in a crystal lattice once a dc electric field is applied was raised by Bloch [31] and Zener [32]. When electrons in crystalline potentials are subject to uniform external fields, Bloch predicted that the quantum coherence properties of the electrons would prevent their transport. He showed that the electrons are dynamically localized and undergo periodic oscillations in space. This effect is nonintuitive: One observes periodic dynamics in contrast to the acceleration towards infinity that would be expected due to the dc field that violates the periodic structure. It leads to the appearance of localized modes (Wannier-Stark states) with equidistant wave-number spacing (Wannier-Stark ladder), that do not

*IlayLevie@gmail.com
†Gregory_Slepyan@yahoo.com

undergo diffraction [33,34]. The BO frequency is $\Omega_B = eaE_{\rm dc}$ where e is electron charge, a is the lattice period, and $E_{\rm dc}$ is the dc field value [25,36]. Remarkably, BOs manifest the wave properties of the electrons, and therefore appear in other types of waves arising in tilted periodic potentials. Inspired by the technological achievements in semiconductor growth at the end of the 20th century, similar phenomena were found in other physical systems, e.g., electronic wave packets in semiconductor superlattices [37,38], cold atoms in optical lattices [39,40], light beams in periodic structures [40–42], and waveguide arrays with linearly varying propagation constants [43,44] (optical BO). It was shown [45] that BOs are able to manifest themselves in quantum optics too: When photons in N-particle entangled state $N00N$ paths undergo Bloch oscillations, they exhibit a periodic transition between spatially bunched and antibunched states. The period of the bunching-antibunching oscillation is N times faster than the period of the photon density oscillation, which signifies their unique coherence properties. Recent progress in fabrication of waveguide lattices, photon-number resolving detectors, and photonic entangled-state sources [46,47] have made experimental observation of the BO within reach [48]. Despite their apparent simplicity, the dynamics of quantum particles in periodic structures turns out to be quite surprising. This is due to the interactions between different physical mechanisms. As an example, we can take an array driven by dc and ac linear (in x) electric fields simultaneously: $V(x,t) = -x[E_0 + E_1\cos(\omega t + \varphi)]$, where $V(x,t)$ is the total applied potential, E_0, E_1 are given constant amplitudes, and φ is a constant phase. A resonant condition $\omega \approx \Omega_B$ results in a beat between the Bloch cycle and the drive, causing a drastic change in the particle motion. On top of the BO, the intraband motion shows a much stronger spatial oscillation that extends over hundreds of lattice cells [49]. These "super-Bloch oscillations" are similar to the motion of normal BO, except being rescaled in space and time. In yet another area, several recent studies [48,50–55] have been made on the dynamics of cold atoms in optical lattices subject to potential ac field forcing; the theoretically predicted renormalization of the tunneling current amplitudes [56] has been verified experimentally.

The subject of this paper is the synthesis of the BO with the RO. We consider a lattice of two-level fermionic systems driven by both dc and ac (optical) electric fields. A resonant condition is $\omega \approx \omega_0$, where ω_0 is the interlevel transition frequency. In contrast with super-Bloch oscillations, the motion here results from the combined dynamics of intraband and interband transitions called the Rabi-Bloch oscillations (RBOs). The total current is the sum of the low-frequency component (tunneling) and the high-frequency component (optical transitions). The total field at the chain axis $\mathbf{E}(x,t) = -\mathbf{e}(\partial V_{\rm dc}/\partial x) + \mathbf{E_0}\cos(\omega t - kx + \varphi)$, where $\mathbf{e}$ is a unit vector along the atomic chain, k is a component of the wave vector along the chain axis, $\mathbf{E_0}$ is the ac field amplitude, and $V_{\rm dc}$ is the static potential. The ac field represents the wave, traveling over the chain. This wave propagation results in a combined effective lattice, produced both in space and time. This lattice manifests itself in strong and repeated interactions between the RO and BO in spite of their strongly different frequency ranges. These interactions, considered in detail below, represent the main line of the results of our paper. A simplified RBO scenario was considered in [57], however, with the ac field assumed to be homogeneous along the chain ($k = 0$), which corresponds to the effective lattice in time only and stops short of accounting for the main part of the effects.

It is well known that a coherent superposition of atomic states in three-level atoms in a Λ configuration is responsible for such interesting phenomena as coherent trapping [58]. These atoms are effectively transparent to the incident field and have important applications such as lasing without inversion, refractive index enhancement in a nonabsorbing medium, and electromagnetically induced transparency [58]. As shown in this paper, similar states exist in the chains of two-level atoms. The role of destructive quantum interference between two lower states in this case is in generating interatomic tunneling. It is shown that RBOs for such type of states differ in a number of features.

Our paper is organized in the following way. In Sec. II, the model system is introduced and equations of its dynamical behavior are derived. Numerical results for inversion, tunneling current, and displacement current are presented and discussed in Sec. III from a physical point of view. In Sec. IV, the validity of the rotating-wave approximation (RWA) is analyzed in comparison with the above analysis. In Sec. V the RBO scenario for the coherently trapped states is investigated. Finally, the main results and outlook problems are described in Sec. VI.

II. MODEL

Let us consider a one-dimensional (1D) structure of identical atoms uniformly distributed over linear lattice points with period a; see Fig. 1(a). Each atom is considered a two-level Fermion system with transition frequency ω_0 [Fig. 1(b)]. For brevity, we refer to the arbitrary two-level quantum object as an "atom" regardless of its physical nature, e.g., quantum dot (QD), polar molecule, trapped ion, etc. The location of the atoms in the lattice points is determined by the radius vector $\mathbf{R}_j = \mathbf{e}ja$; $j = 0,1,\ldots,N$; N is a number of atoms; $\mathbf{e}$ is the unit vector over the lattice. The index j thus completely determines the atom location. We assume the atoms to be coupled via interatomic tunneling. The chain is driven by an electrostatic (dc) field directed along its axis while simultaneously interacting with a monochromatic electromagnetic (ac) field. We will consider the case of dipole interaction in the regime of strong coupling and assume the resonant condition $\omega_0 \approx \omega$ to be fulfilled. The system under consideration exhibits complex single-particle RBO, for which the theoretical framework is introduced below.

A. Unperturbed Hamiltonian in Wannier basis

The analysis that follows is based on the single-particle Hamilton approach with the Hamiltonian $\hat{H} = \hat{H}_0 + \hat{H}_I$, where

$$\hat{H}_0 = \frac{\hat{\mathbf{p}}^2}{2m} + V(\mathbf{r}) \tag{1}$$

is the component of free-electron movement in the chain associated with the interatomic tunneling, which is described by the periodic potential $V(\mathbf{r})$. The excited and ground states of the atoms here and thereafter will be denoted a and b, respectively. The eigenmodes of the Hamiltonian (1) are two Bloch modes corresponding to the valence (b) and conductive

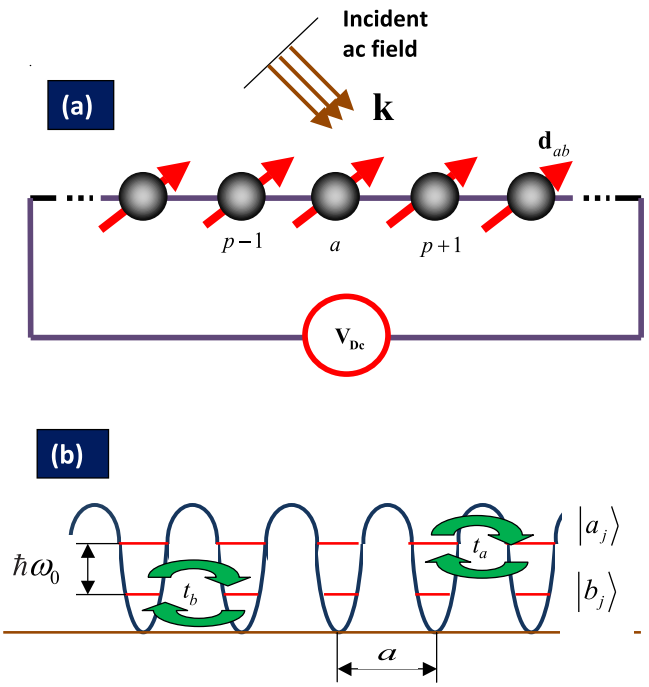

FIG. 1. (a) General illustration of the periodic two-level atomic chain used as a model, indicating RBO. It is excited with obliquely incident ac field in the strong coupling regime and driven with dc voltage applied at the ends. The dipole moments (red arrows) are identical and oriented arbitrarily with respect to the axis. (b) The electrons are localized inside the quantum wells which are separated by potential barriers of identical form and value. The neighboring atoms are coupled via interatomic tunneling with different values of penetration $t_{a,b}$ at the ground and excited states (green arrows). Ground and excited energy levels of single two-level atom separated by the transition energy $\hbar\omega_0$.

(a) zones and denoted as $\psi_{n,h}(\mathbf{r}) = |n,h\rangle$, $n = a,b,h$ being a scalar quasimomentum directed along the chain. The second component of the Hamiltonian,

$$\hat{H}_I = -e\mathbf{E}(\mathbf{r},t)\cdot\hat{\mathbf{r}}, \tag{2}$$

describes the dipole interaction of the chain with the total (dc and ac) electromagnetic field; $\hat{\mathbf{r}}$ is the operator of electron position in the chain.

Because the electrons are strongly confined inside the atoms, we will use as a basis Wannier functions $\phi_{n,\mathbf{R}_j}(\mathbf{r}) = |n,\mathbf{R}_j\rangle$ [59], defined as a linear combinations of Bloch modes $\psi_{n,h}(\mathbf{r})$:

$$\phi_{n,\mathbf{R}_j}(\mathbf{r}) = \frac{1}{\sqrt{N}}\sum_h e^{-ih(\mathbf{e}\cdot\mathbf{R}_j)}\psi_{n,h}(\mathbf{r}), \tag{3}$$

where $\mathbf{e}$ is the unit vector along the chain, $\mathbf{R}_j = \mathbf{e}ja$. Let us mention some properties of Wannier functions, which are important for our analysis. A typical Wannier function $\phi_{n,\mathbf{R}_j}(\mathbf{r})$ is strongly localized within the jth atom. Inversion of Eq. (3) gives the expression of Bloch states in terms of the Wannier functions:

$$\psi_{n,h}(\mathbf{r}) = \frac{1}{\sqrt{N}}\sum_{\mathbf{R}_j} e^{ih(\mathbf{e}\cdot\mathbf{R}_j)}\phi_{n,\mathbf{R}_j}(\mathbf{r}-\mathbf{R}_j). \tag{4}$$

Wannier functions at different locations are related via the relationship $\phi_{n,\mathbf{R}_j}(\mathbf{r}) = \phi_{n,\mathbf{R}_j+\mathbf{R}_l}(\mathbf{r}+\mathbf{R}_l)$ and satisfy the orthogonality relation $\langle n,\mathbf{R}_j\,|\,m,\mathbf{R}_l\rangle = \delta_{mn}\delta_{\mathbf{R}_j,\mathbf{R}_l}$.

The first step of our analysis is the representation of the Hamiltonian (1) in the Wannier basis. Upon projecting $\hat{H}_0$ on the Bloch modes and using (4), we obtain the dispersion law for a free-tunneling electron in the following form:

$$\varepsilon_n(h) = \langle n,h|\hat{H}_0|n,h\rangle = \frac{1}{N}\sum_{\mathbf{R}_j,\mathbf{R}_l} e^{-ih\mathbf{e}\cdot(\mathbf{R}_j-\mathbf{R}_l)}\langle n,\mathbf{R}_j|\hat{H}_0|n,\mathbf{R}_l\rangle. \tag{5}$$

Introducing the shorthand notation $t_n(\mathbf{R})$ via

$$\langle n,\mathbf{R}_j|\hat{H}_0|n,\mathbf{R}_l\rangle = \begin{cases}\varepsilon_n(0), & j = l\\ t_n(\mathbf{R}_j-\mathbf{R}_l), & j\neq l\end{cases}, \tag{6}$$

we can rewrite (5) in the following form:

$$\varepsilon_n(h) = \varepsilon_n(0) + \frac{1}{N}\sum_{\mathbf{R}_j,\mathbf{R}_l,j\neq l} e^{-ih\mathbf{e}\cdot(\mathbf{R}_j-\mathbf{R}_l)}t_n(\mathbf{R}_j-\mathbf{R}_l), \tag{7}$$

where $t_{a,b}(\mathbf{R}_j-\mathbf{R}_l) = t^*_{a,b}(\mathbf{R}_l-\mathbf{R}_j)$ are the matrix elements of the free Hamiltonian with the Wannier basis for functions localized at the cells numbered j,l, respectively. The Hamiltonian (1) may be presented with the Wannier basis in the form of a block diagonal matrix,

$$\hat{H}_0 = \begin{pmatrix}\hat{H}_{0a} & 0\\ 0 & \hat{H}_{0b}\end{pmatrix}, \tag{8}$$

with the submatrices along the diagonal being

$$\hat{H}_{0n} = \varepsilon_n(0)\sum_{\mathbf{R}_j}|n,\mathbf{R}_j\rangle\langle n,\mathbf{R}_j| + \sum_{\mathbf{R}_j,\mathbf{R}_l,j\neq l} t_n(\mathbf{R}_j-\mathbf{R}_l)|n,\mathbf{R}_l\rangle\langle n,\mathbf{R}_j|. \tag{9}$$

We now assume the tight-binding approximation where tunneling coupling exists only between the neighboring atoms. Thus, we can omit the spatial arguments in the tunneling matrix elements: $t_{a,b}(\mathbf{R}_j-\mathbf{R}_{j+1}) = t_{a,b}$, $t_{a,b}(\mathbf{R}_j-\mathbf{R}_{j-1}) = t^*_{a,b}$, and redenote Wannier functions as $|n,\mathbf{R}_j\rangle \to |n,j\rangle$. The Hamiltonian (8), subject to (9), then reads

$$\hat{H}_0 = \varepsilon_b(0)\sum_j|b,j\rangle\langle b,j| + \varepsilon_a(0)\sum_j|a,j\rangle\langle a,j| + \sum_j(t_b|b,j\rangle\langle b,j+1| + t^*_b|b,j\rangle\langle b,j-1|) + \sum_j(t_a|a,j\rangle\langle a,j+1| + t^*_a|a,j\rangle\langle a,j-1|). \tag{10}$$

The Hamiltonian (10) describes the free (without dc and ac fields) electron motion in the periodic system with potential wells separated by the potential barriers. The electron is localized inside a well at one of the two states (ground or excited). This localization is not perfect due to the finite value of the barrier potential. As a result, the Wannier functions for ground and excited states localized inside the given well are

coupled with the correspondent functions in the neighboring wells. This coupling describes the interatomic tunneling. It is characterized by the transparence of the potential barrier at the given state and correspondent values of penetration factors $t_{a,b}$. The tunneling leads to the tailing of discrete levels into the energy zones with the widths defined by the correspondent penetration factors. The different scenarios of the electron tunneling will be considered in this paper. For the first one, the ground-state energy lies near the bottom of the quantum well. Therefore, its penetration over the barrier becomes difficult ($t_b \approx 0$) and the width of the zone is small. Thus the dominant part of the tunneling current flows over the excited zone. The second case corresponds to the atom appearing in the coherent superposition of excited states with very high principal quantum numbers (Rydberg atom [60]). The energies of the two states are placed near the edge of the potential barrier, and the probabilities of their tunneling are approximately the same. The widths of the two zones as well as their contributions to the total tunneling current are commensurable.

B. Interaction Hamiltonian in Wannier basis

Let us proceed with the calculation of the matrix elements $\langle m,l|\hat{H}_I|n,j\rangle$ of the interaction Hamiltonian (2). Such a motion, being a combined interband transition and interatomic tunneling through the potential barrier, requires values of energy that are high enough for the probability to become negligibly small. Thus, for the simultaneous inequalities $m \neq n, l \neq j$ we have $\langle m,l|\hat{H}_I|n,j\rangle \approx 0$. We assume the intra-atomic confinement sufficiently high, such that the electric field is approximately homogeneous over the support area of the localized Wannier function. Hence we have

$$\langle m,j|\hat{H}_I|n,j\rangle \approx -e\mathbf{E}(ja,t)\cdot\langle m,j|\hat{\mathbf{r}}_j|n,j\rangle \tag{11}$$

with the electric field

$$\mathbf{E}(j,t) \approx \mathbf{E}_{\rm dc} + \omega A_0 \mathbf{u}\cos[(\mathbf{k}\cdot\mathbf{e})ja - \omega t], \tag{12}$$

where the first term is a bias dc field; the second one is the incident plane wave; $\mathbf{E}_{\rm dc}$ and A_0 are constant values; $\mathbf{u}$ is the unit vector of polarization; $\mathbf{k}$ is the wave vector. The plane wave in the general case propagates obliquely with respect to the chain axis ($\mathbf{k}\cdot\mathbf{e} \neq 0$); therefore the electron moves in a spatial-temporal lattice produced by the second term in Eq. (12). Let us shift the origin for a given j to the center of the jth atom via the relation $\hat{\mathbf{r}}_j = \mathbf{R}_j\hat{I} + \hat{\mathbf{r}}'$. Using the orthogonality of the Wannier functions for different bands, we have $\langle m,j|\hat{\mathbf{r}}_j|n,j\rangle = \mathbf{R}_j\delta_{mn} + \langle m,j|\hat{\mathbf{r}}'|n,j\rangle$, where $\mathbf{R}_j$ was defined before (3) and δ_{mn} is the Kronecker delta. This makes (11)

$$\langle m,j|\hat{H}_I|n,j\rangle = -\mathbf{E}(ja,t)\cdot(e\mathbf{R}_j\delta_{mn} + \mathbf{d}_{mn}), \tag{13}$$

where

$$\mathbf{d}_{mn} = e\langle m,j|\hat{\mathbf{r}}'|n,j\rangle. \tag{14}$$

It is important to note that the coefficients (14) are position independent. The first term in (13) consists of the diagonal elements of the Hamiltonian (11). It describes BO and super-Bloch oscillations governed by the intraband motions at the excited and ground states, respectively [36,49]. The diagonal elements of the second term in (13) vanish for real atoms (excluding the hydrogen atom) due to $d_{aa,bb} \to 0$ on the assumption of symmetry properties [61]. However, they may be nonzero for cases such as artificial atoms with broken inversion symmetry [62].

Another type of matrix element required for our analysis couples the electrons of neighboring atoms in the same band via the ac field (this is the tunneling photon assistance):

$$\langle n,j|\hat{H}_I|n,j+1\rangle = -e\omega A_0 d_{nj}(t), \tag{15}$$

where $d_{nj}(t) = \langle n,j|(\hat{\mathbf{r}}\cdot\mathbf{u})\cos[(\mathbf{k}\cdot\hat{\mathbf{r}}) - \omega t]|n,j+1\rangle$. Using the homogeneity of the ac field over the atom size, we transform it approximately to

$$d_{nj}(t) \approx \cos[(\mathbf{k}\cdot\mathbf{e})ja - \omega t]\langle n,j|(\hat{\mathbf{r}}\cdot\mathbf{u})|n,j+1\rangle. \tag{16}$$

C. Equations of motion

Our starting point is the Schrödinger equation $i\hbar\partial_t|\psi\rangle = \hat{H}|\psi\rangle$ with the total Hamiltonian being

$$\begin{aligned}\hat{H} = {}& \varepsilon_b(0)\sum_j |b,j\rangle\langle b,j| + \varepsilon_a(0)\sum_j |a,j\rangle\langle a,j| + \sum_j (t_b|b,j\rangle\langle b,j+1| + t_b^*|b,j\rangle\langle b,j-1|)\\ &+ \sum_j (t_a|a,j\rangle\langle a,j+1| + t_a^*|a,j\rangle\langle a,j-1|) - \sum_j \mathbf{E}(j,t)\cdot(e\mathbf{R}_j + \mathbf{d}_{bb})|b,j\rangle\langle b,j|\\ &- \sum_j \mathbf{E}(j,t)\cdot(e\mathbf{R}_j + \mathbf{d}_{aa})|a,j\rangle\langle a,j| - \omega A_0\sum_j d_{bj}(t)|b,j\rangle\langle b,j+1| - \omega A_0\sum_j d_{aj}(t)|a,j\rangle\langle a,j+1|\\ &- \omega A_0\sum_j d_{bj}^*(t)|b,j\rangle\langle b,j-1| - \omega A_0\sum_j d_{aj}^*(t)|a,j\rangle\langle a,j-1| - \sum_j \mathbf{E}(j,t)\cdot\mathbf{d}_{ab}|a,j\rangle\langle b,j| - \sum_j \mathbf{E}(j,t)\cdot\mathbf{d}_{ba}|b,j\rangle\langle a,j|,\end{aligned} \tag{17}$$

which follows from (10) and (13)–(16). We present the required wave function as a superposition of Wannier functions,

$$|\psi(t)\rangle = \sum_j \{a_j(t)|a,j\rangle + b_j(t)|b,j\rangle\}, \tag{18}$$

with unknown coefficients $a_j(t),b_j(t)$. Using the orthogonality of the Wannier functions mentioned above, we obtain the following system of coupled differential equations for the probability amplitudes $a_j(t),b_j(t)$:

$$i\hbar\frac{\partial a_j}{\partial t} = [\varepsilon_0 + \delta\varepsilon - \mathbf{E}(j,t)\cdot(e\mathbf{R}_j + \mathbf{d}_{aa})]a_j + [t_a - \omega A_0 d_{aj}(t)]a_{j+1} + [t_a^* - \omega A_0 d_{aj}^*(t)]a_{j-1} - \mathbf{E}(j,t)\cdot\mathbf{d}_{ab}b_j, \quad (19)$$

$$i\hbar\frac{\partial b_j}{\partial t} = [\varepsilon_0 - \delta\varepsilon - \mathbf{E}(j,t)\cdot(e\mathbf{R}_j + \mathbf{d}_{bb})]b_j + [t_b - \omega A_0 d_{bj}(t)]b_{j+1} + [t_b^* - \omega A_0 d_{bj}^*(t)]b_{j-1} - \mathbf{E}(j,t)\cdot\mathbf{d}_{ba}a_j, \quad (20)$$

where $\varepsilon_0 = [\varepsilon_a(0) + \varepsilon_b(0)]/2$, $\delta\varepsilon = [\varepsilon_a(0) - \varepsilon_b(0)]/2$.

The system (19) and (20) represents the framework for investigation of RBO. It is analytically unsolvable; therefore it will be integrated numerically. The numerical procedure is free from some conventional approximations such as RWA [63]. The coefficients $t_{a,b}$,$d_{aa,bb}$,$d_{aj,bj}$,d_{ab} are considered phenomenological, *a priori* given parameters. It may be instructive to dwell on the physical meaning of the different terms and quantities appearing in the system (19) and (20). The first quantity $2\delta\varepsilon$ is the minimal energy of the optical transition between the valence and conductive bands. It defines the frequency of free interband oscillations in the absence of external electromagnetic (EM) field. The energy benchmark given by the value ε_0 defines the phase factor, which does not support observable values, and thus may be set as $\varepsilon_0 = 0$ [62]. The factor $\mathbf{E}(j,t)\cdot\mathbf{R}_j \cong ja\mathbf{E}(j,t)\cdot\mathbf{e}$ in (19) and (20) describes BOs and super-Bloch oscillations at the excited and ground states, respectively [36,49]. The coefficients $d_{aa,bb}$ vanish for real atoms (excluding the hydrogen atom) on the assumption of symmetry properties [61]. However, they may be nonzero for cases such as semiconductor quantum dots with broken inversion symmetry [62]. This leads to the appearance of an additional line in the spectrum of RO for the single quantum dot [63] and not considered in this paper. The factors $t_{a,b} - \omega A_0 d_{aj,bj}(t)$ describe the coupling between the neighboring atoms (the first term corresponds to direct tunneling; the second one stands for the tunneling photonic assistance). The last terms in (19) and (20) describe coupling between the ground and excited states via the EM field. The value $\Omega_R = (\mathbf{u}\cdot\mathbf{d}_{ab})\omega A_0/\hbar$ may be associated with the Rabi frequency for the chain. It differs from the conventional Rabi frequency defined for individual atom [58], because of the appearance of the Wannier states in (14) instead of atomic orbitals. For the deep atomic levels of the Rabi frequency [58], the conventional Rabi frequency is nonetheless approximated because the deep Wannier states tend to the corresponding atomic orbitals.

The system (19) and (20) may be simplified assuming the atoms to be inversion symmetrical ($\mathbf{d}_{aa} = \mathbf{d}_{bb} = 0$) and neglecting the photon assistance ($d_{aj,bj} \approx 0$). In this case, (19) and (20) become

$$i\hbar\frac{\partial a_j}{\partial t} = (\delta\varepsilon - \mathbf{E}_0\cdot e\mathbf{R}_j)a_j + t_a a_{j+1} + t_a^* a_{j-1} - \mathbf{E}_j(t)\cdot\mathbf{d}_{ab}b_j, \quad (21)$$

$$i\hbar\frac{\partial b_j}{\partial t} = -(\delta\varepsilon + \mathbf{E}_0\cdot e\mathbf{R}_j)b_j + t_b b_{j+1} + t_b^* b_{j-1} - \mathbf{E}_j(t)\cdot\mathbf{d}_{ba}a_j. \quad (22)$$

D. Inversion and electric current

The principal quantities describing the RBO are inversion, tunneling, and dipole currents, expressed in the terms of probability amplitudes, to be calculated from (19) and (20) [or (21) and (22)]. These values are position dependent; therefore we will refer to their densities per unit cell of the chain. The inversion density is

$$w_j(t) = \frac{1}{N}(|a_j|^2 - |b_j|^2). \quad (23)$$

The equation for the tunneling current density is (see detailed derivation in the Appendix)

$$J_{\text{Tunneling},j}(t) = J^{(a)}_{\text{Tunneling},j}(t) + J^{(b)}_{\text{Tunneling},j}(t) = -i\frac{e}{2}t_a[a_{j-1}(t) - a_{j+1}(t)]a_j^*(t) - i\frac{e}{2}t_b[b_{j-1}(t) - b_{j+1}(t)]b_j^*(t) + \text{c.c.} \quad (24)$$

The operator of the dipole current in the Heisenberg picture is $\hat{J}_{\text{Dipole},j}(t) = c\partial\hat{P}_j(t)/\partial t$, where $\hat{P}_j(t)$ is the polarization operator of the atom with number j. In the Schrödinger picture, we obtain $\hat{J}_{\text{Dipole},j} = -i\omega ced_{ab}|a,j\rangle\langle b,j| + \text{H.c.}$, and the observable current reads

$$J_{\text{Dipole},j}(t) = -i\omega ced_{ab}a_j^*(t)b_j(t) + \text{c.c.} \quad (25)$$

III. RESULTS AND DISCUSSION

The system under consideration comprises a large number of physical phenomena. Certain combinations of these phenomena correspond to different physical regimes of RBO dependent on such physical parameters as Bloch frequency Ω_B, Rabi frequency Ω_R, the component of wave vector $k = (\mathbf{k}\cdot\mathbf{e})$ of the incident wave with respect to the chain axis, and tunneling penetration parameters $t_{a,b}$ at the excited and ground states. The case $k = 0$ corresponds to the normal incidence of an external plane wave with respect to the chain axis; therefore the ac field is homogeneous along the chain (this is a standing wave case). The case $k \neq 0$ corresponds to oblique incidence; the ac field oscillates along the chain (now a traveling wave case). Two different regimes of interatomic coupling have been considered. For the first type, the penetration tunneling factors are comparable (taken here as equal for simplicity). For the second case, the tunneling penetration at the excited state strongly exceeds the value at the ground state. For convenience, the different analyzed physical regimes of RBO are presented in Table I.

Let us assume that the system is initially excited with the Gaussian wave packet

$$a_j(0) = ge^{-\frac{(j-j')^2a^2}{\sigma^2}}, \quad (26)$$

$$b_j(0) = 0, \quad (27)$$

where g is a normalization factor, and j',σ are the position of the Gaussian center and the effective Gaussian width,

TABLE I. Classification of possible interaction types and correspondent dynamics in the 1D chain with RBO. $k = \mathbf{k} \cdot \mathbf{e}$.

Variant	Type of interaction	Type of dynamics
(a)	$E_{\rm dc} \neq 0, E_{\rm ac} = 0$ $t_a = t_b$	BO [35]; the tunneling penetrations at the two levels are equal
(b)	$E_{\rm dc} = 0, E_{\rm ac} \neq 0, k = 0$ $t_a = t_b$	RO [58]; the tunneling penetrations at the two levels are equal
(c)	$E_{\rm dc} = 0, E_{\rm ac} \neq 0, k \neq 0$ $t_a = t_b$	Rabi waves [23–28]; the tunneling penetrations at the two levels are equal
(d)	$E_{\rm dc} \neq 0, E_{\rm ac} \neq 0, k = 0$ $t_a = t_b$	RBO in the standing ac field; the tunneling penetrations at the two levels are equal
(e)	$E_{\rm dc} \neq 0, E_{\rm ac} \neq 0, k \neq 0,$ $t_a = t_b$	RBO in the traveling wave; the tunneling penetrations at the two levels are equal
(f)	$E_{\rm dc} \neq 0, E_{\rm ac} \neq 0, k = 0$ $t_a \gg t_b$	RBO in the standing ac field; the tunneling penetration at the excited level strongly exceeds the tunneling penetration at the ground level

respectively. Here we will present the results, obtained via the numerical solution of Eqs. (21) and (22).

Numerical modeling shows that the system dynamics comprises the superposition of two phenomena: The first one is the interatomic intraband transitions by electron tunneling; the second one is the intra-atomic interband quantum transitions. Because these interaction types belong in different frequency ranges, the total motion does not add up to their simple linear superposition. It is characterized by their strong mutual influence, which produces nontrivial dynamics and qualitative features of the spectra. The reason for it is the diffraction by the spatial-temporal lattice induced by the ac field, i.e., the factor $\cos[(\mathbf{k} \cdot \mathbf{e})ja - \omega t]$ in the last terms of (21) and (22).

Figures 2 and 3 shows the temporal behavior of the inversion density. Let us start with two illustrative limiting cases: In the first case, $A_0 = 0$ (i.e., no ac field and hence no RO). This case corresponds to the ordinary BO, where the inversion oscillates at the lower Bloch frequency Ω_B [35] [Fig. 2(a)]. The oscillations are approximately monochromatic: The values of the high harmonics are rather weak; see Fig. 4(a). For the second case, $\mathbf{E}_0 = 0$. Here, the driven dc field is absent [Fig. 2(b)]. This case corresponds to the ordinary RO [57]; the inversion oscillates monochromatically at the higher Rabi frequency Ω_R. Figure 2(d) shows the first example of RBO, where both ac and dc fields are present. The ac field is normally incident with respect to the chain axis $[k = (\mathbf{k} \cdot \mathbf{e}) = 0]$; therefore the ac field is homogeneous along this axis. This is the case of a temporal lattice, in which the total motion adds up to a linear superposition of RO and BO. In other words, the ROs become modulated by the Bloch frequency. The inversion spectrum is transformed to the triplet in Fig. 4(d), with a central line at $\omega = \Omega_R$ and two side bands at $\omega = \Omega_R \pm \Omega_B$.

The qualitative behavior of motion dramatically changes for the spatial-temporal lattice, where the ac field is obliquely incident ($k \neq 0$); see Figs. 2(c) and 2(e). The initial Gaussian packet rapidly decays and breaks into a set of rather small subpackets; thus the state becomes a strongly oscillating packet with an approximately Gaussian envelope; See Fig. 3. This is a manifestation of the diffraction mentioned above, along with the spatial oscillations corresponding to the Floquet harmonics. As a result, the BO is accompanied with a motion of the subpackets relative to one another. This motion leads to appearance of additional spectral lines [Figs. 4(c) and 4(e)] whose amplitudes are comparable to the main one. Figure 2(d) corresponds, for example, to the case of a Rydberg atom where two sidebands appear in excited states with very high principal quantum numbers [62]. As a result, the energies

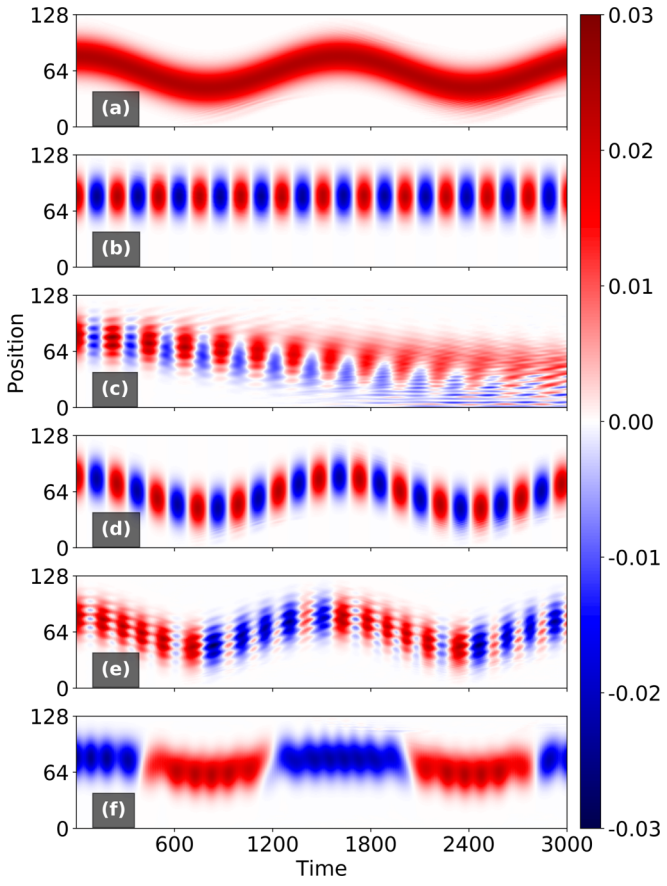

FIG. 2. Space-time distribution of inversion density. Here, (a–f) notation corresponds to Table I. Here, the quantum transition frequency is taken as the frequency unit, $\Omega_B = 3.9 \times 10^{-3}$ (corresponds to $E_{\rm dc} = 1.95\,{\rm kV/cm}$), $\Omega_R = 2.5 \times 10^{-2}$, $t_a = 3.5 \times 10^{-2}$, interatomic distance $a = 20\,{\rm nm}$. The initial state of the chain is an excited single Gaussian wave packet. Gaussian initial position and width are $p' = 80$, $g = 20$, respectively, $ka = -0.624$. Number of the atoms, $N = 128$.

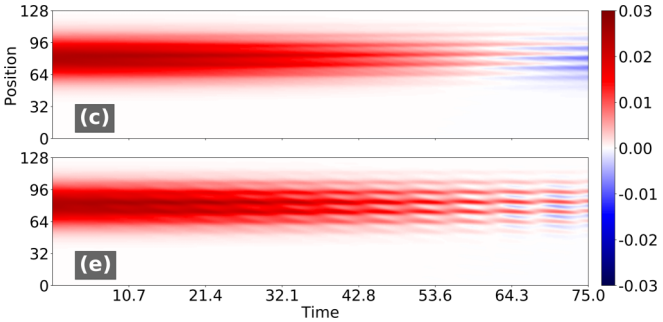

FIG. 3. Space-time distribution of inversion density for short times. Here, (c,e) notation corresponds to Table I. Spatial beatings correspond to the Floquet harmonics in the electron diffraction by the lattice induced by the ac field at the case of oblique incidence. As a result, the initial single Gaussian decays into the set of subpackets, which synchronously move and coherently oscillate in the large-time regime (Fig. 2). All parameters are identical to Fig. 2.

of the two states are placed near the edge of the potential barrier, and the probabilities of their tunneling are approximately the same (taken, for simplicity, as exactly equal, $t_a = t_b$).

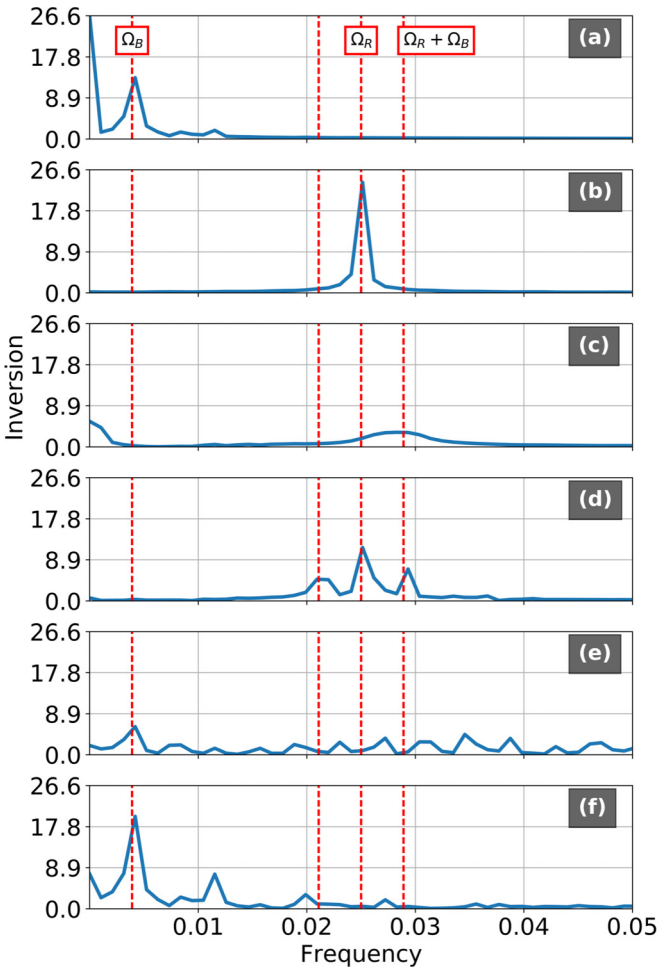

FIG. 4. Frequency spectra of the inversion density. Here, (a–f) notation corresponds to Table I. The quantum transition frequency is taken as the unit. All parameters are identical to Fig. 2. For better discrimination, the results presented in this figure are multiplied by the factor 10^{-2}.

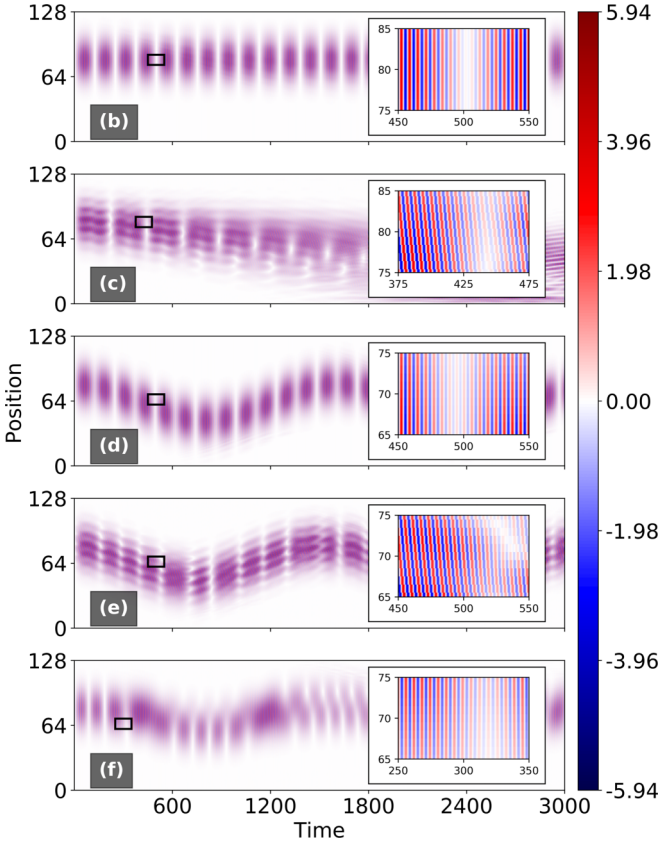

FIG. 5. Space-time distribution of the density of dipole current. Here, (b–f) notation corresponds to Table I. All parameters are identical to Fig. 2. Inserts show scaled-up space-time distribution in the areas marked via the black rectangles at the main panels. For better discrimination, the results presented in this figure are multiplied by the factor 10^4.

Figure 2(f) corresponds to an atom excited in the state with a weak quantum number. Therefore, the ground-state energy lies near the bottom of the quantum box. Therefore, its penetration over the barrier becomes difficult ($t_b \approx 0$). This effect manifests itself in the difference between the inversion dynamics: The blue-colored regions in Fig. 2(f) show oscillations in time, however, without spatial motion. The reason is in the negative inversion, which corresponds to the ground state with a vanishing tunneling probability. Figures 5 and 6 show the temporal dynamics and the spectra of the dipole current, respectively. Their qualitative behavior agrees with the corresponding inversion features. Figure 6(b) presents the conventional case of RO, characterized by the spectrum of the dipole current as a duplet with separating value $2\Omega_R$ with respect to the frequency of optical transition. The central line is absent due to zero detuning (exact resonance). For RBOs with $k = 0$ [Fig. 6(d)], the independent spectrum lines are transformed into triplets with double-Bloch splitting. The next important peculiarity is the appearance of a central triplet with rather small amplitude even in the exact resonance case. For RBOs with $k \neq 0$ [Figs. 6(c)–6(e)] the sideband triplets are transformed into a multiplicity of lines with the Bloch frequency serving in the capacity of the interline separation. For the Rydberg-atomic case [Figs. 6(d) and 6(e)] the amplitude of the central triplet is enhanced and has become comparable with additional lines.

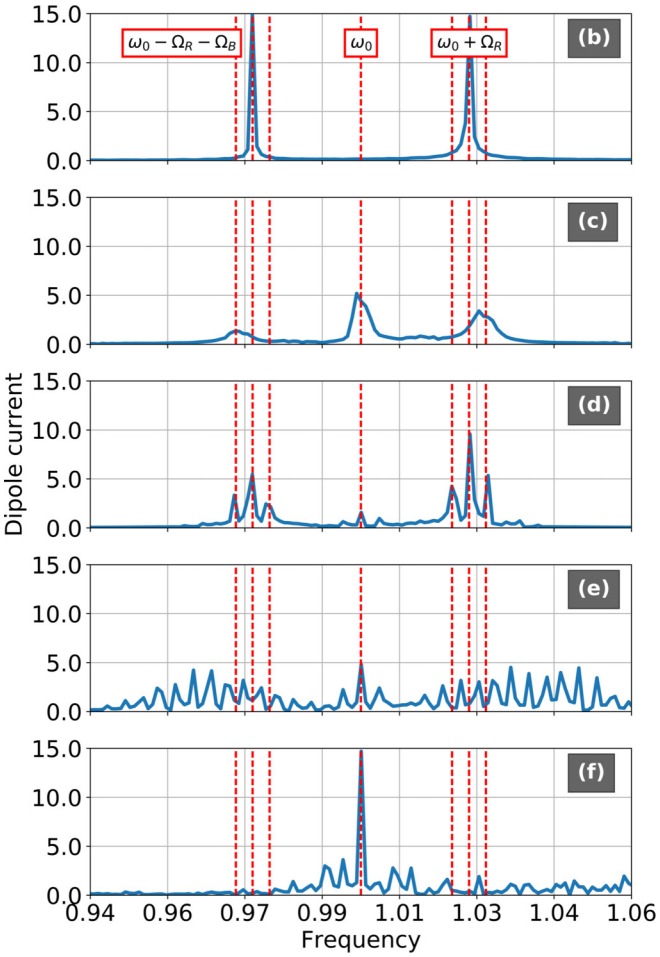

FIG. 6. Frequency spectra of dipole current. Here, (b–f) notation corresponds to Table I. The quantum transition frequency is taken as the unit. All other parameters are identical to Fig. 2.

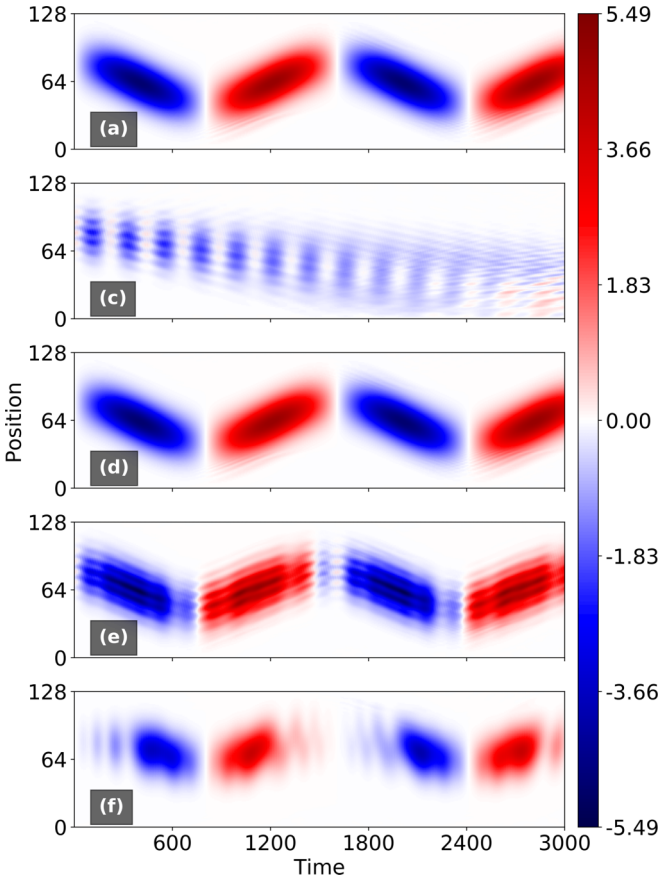

FIG. 7. Space-time distribution of the tunnel current density. Here, (a,c–f) notation corresponds to Table I. All parameters are identical to Fig. 2. For better discrimination, the results presented in this figure are multiplied by the factor 10^4.

For the case of deep ground state [Fig. 6(f)], the RO are suppressed while the central triplet has become dominant.

As one more example of the similar scenario of complex dynamics, the coherent control in molecular complexes of a donor-bridge-acceptor type may be considered [64]. Such control is induced by resonances between the RO driven by a pumping laser field, and the bridge mediated tunneling oscillations between the lowest unoccupied molecular orbitals of the donor and acceptor. These tunneling oscillations may be associated with BO in atomic chains. The frequency of intramolecular oscillations in [64] should be identified as a Bloch frequency Ω_B in the system under consideration. In this case, the resonant lines in Figs. 6(d)–6(f) agree with the resonance condition in [64].

Figure 7 demonstrates the dynamics of the tunnel current. Let us note that it is again in agreement with the behavior of the inversion. In particular, in Fig. 7(f), we observe cells of zero tunnel current in the area of RBO, in contrast with Fig. 7(a). Such cells represent the areas of negative inversion and stopped electron motion. The spectrum of the tunnel current (Fig. 8) consists of a dc component, the main Bloch component and high-order Bloch lines. In all cases, the second Bloch harmonic is high; its amplitude is comparable with the main line. The mutual RO and BO influence manifests itself in the enhancement of high-order harmonics in the tunnel current [Figs. 8(e) and 8(f)].

IV. ROTATING-WAVE APPROXIMATION

For the sake of comparison, we now present a development of the physics of periodic low-dimensional lattices and their interaction with EM field using some conventional simplifications. These include the tight-binding approximation and the RWA [58]. In spite of the fact that these models have been tested exhaustively in the past, their validity becomes questionable when new physical factors and corresponding degrees of freedom are introduced. For this reason, testing of these methods is of continued interest. As an instructive example for the failure of such models, we can note the phenomenon of virtual photons [63], which qualitatively changes the long-term dynamics of the collective spontaneous emission. This phenomenon cannot be described by the RWA. The Rabi-wave theory [23–28], although based on the RWA, may not be valid when adding dc field (and BO). Therefore, although the model developed in this paper is free of RWA, special numerical experiments with RWA are presented in this section and compared with direct calculations, with the objective of identifying sources of potential errors.

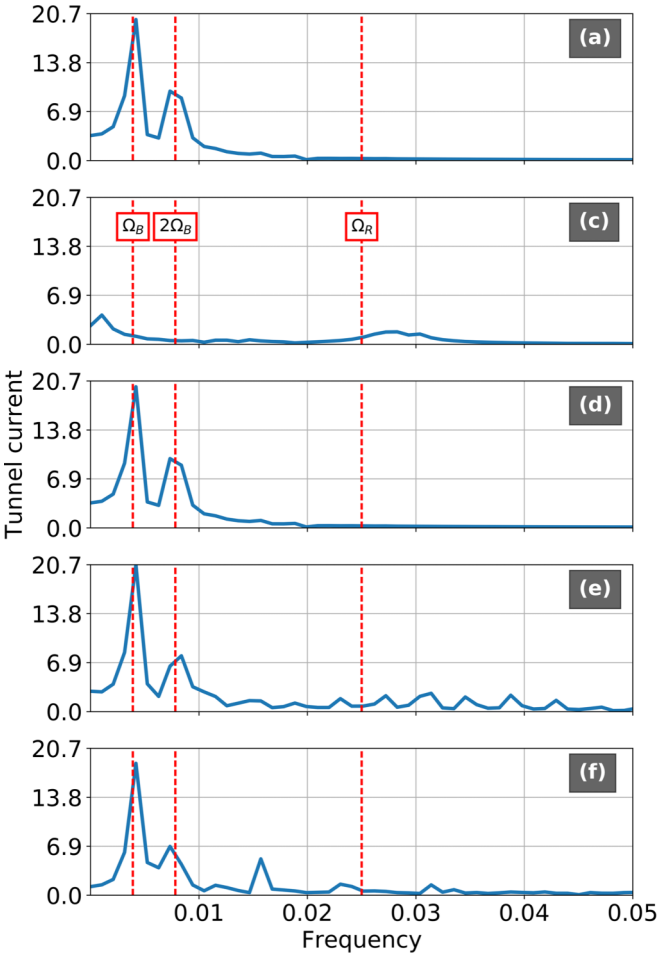

FIG. 8. Frequency spectra of tunnel current. Here, (b–f) notation corresponds to Table I. The quantum transition frequency is taken as the unit. All other parameters are identical to Fig. 2.

The RWA is based on neglecting highly oscillating terms [58]. Applying this approximation to (19) and (20), we have

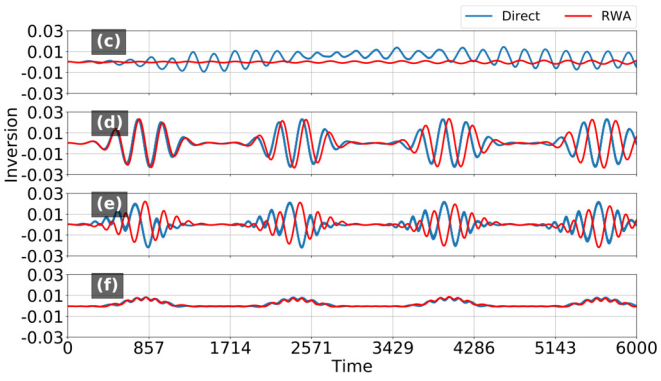

FIG. 9. Plot of inversion against a dimensionless time at the atom with number 40. Here, (c–f) notation corresponds to Table I. Direct solution: blue line; RWA solution: red line. The initial state of the chain is an excited single Gaussian wave packet. All units and parameters are identical to Fig. 2. One can see that RWA correctly reproduces the qualitative dynamics of inversion, but allows rather high inaccuracies in detail description.

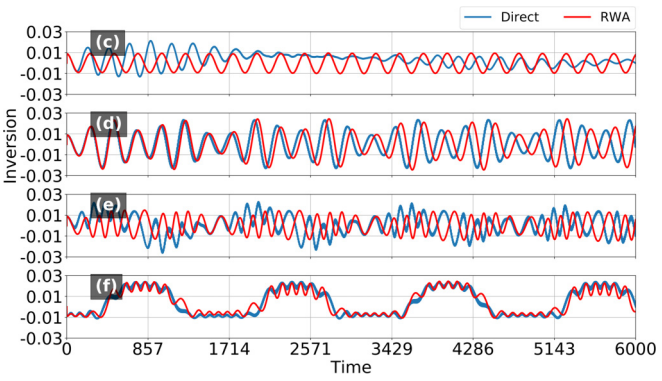

FIG. 10. Plot of inversion against a dimensionless time at the atom with number 60. Here, (c–f) notation corresponds to Table I. Direct solution: blue line; RWA solution: red line. The initial state of the chain is an excited single Gaussian wave packet. All units and parameters are identical to Fig. 2.

the following form:

$$i\hbar\frac{\partial a_j}{\partial t} = (\delta\varepsilon - \mathbf{E}_0\cdot e\mathbf{R}_j)a_j + t_a a_{j+1} + t_a^* a_{j-1} - \frac{1}{2}\omega A_0(\mathbf{u}\cdot\mathbf{d}_{ab})e^{i[(\mathbf{k}\cdot\mathbf{e})ja-\omega t]}b_j, \quad (28)$$

$$i\hbar\frac{\partial b_j}{\partial t} = -(\delta\varepsilon + \mathbf{E}_0\cdot e\mathbf{R}_j)b_j + t_b b_{j+1} + t_b^* b_{j-1} - \frac{1}{2}\omega A_0(\mathbf{u}\cdot\mathbf{d}_{ba})e^{-i[(\mathbf{k}\cdot\mathbf{e})ja-\omega t]}a_j. \quad (29)$$

Results of the RWA compared with a direct solution for the inversion dynamics are shown in Figs. 9–11. Two different scenarios are observed for different RBO regimes. The first one corresponds to oscillations with Rabi frequency and smoothly various envelopes. The second one exhibits the collapse-revival picture similar to the Jaynes-Cummings dynamics [58], though the electromagnetic field is of classical origin. The reason for this is that in both cases the RO spectrum is multiharmonic independently of its physical origin. One can see that the RWA correctly reproduces the qualitative temporal behavior of inversion (in the first or second type of the aforementioned sce-

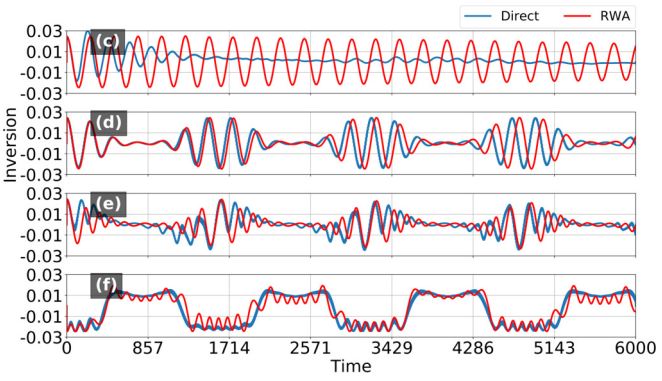

FIG. 11. Plot of inversion against a dimensionless time at the atom with number 80. Here, (c–f) notation corresponds to Table I. Direct solution: blue line; RWA solution: red line. The initial state of the chain is an excited single Gaussian wave packet. All units and parameters are identical to Fig. 2.

narios), but allows for rather high inaccuracies in the detailed description, in contrast to the single Rabi oscillator [58].

V. RABI-BLOCH OSCILLATIONS AND COHERENT TRAPPING

We begin our analysis with the simplest analytical model based on the system (28) and (29), solving it in the limits of the RWA for the case $\Omega_B = 0$. We assume for simplicity that the exact resonance condition $\omega = 2\delta\varepsilon/\hbar$ has been fulfilled. The steady-state solution for the chain with oscillations at this transition frequency is

$$|\Psi(t)\rangle = \frac{1}{\sqrt{N}} \sum_j \left\{ u e^{-i\left(\frac{\delta\varepsilon}{\hbar}t - \frac{kja}{2}\right)} |a,j\rangle + v e^{i\left(\frac{\delta\varepsilon}{\hbar}t - \frac{kja}{2}\right)} |b,j\rangle \right\} e^{ihja}, \tag{30}$$

where u, v are unknown constant amplitudes normalized as $|u|^2 + |v|^2 = 1$, and h is the unknown wave number. Substituting (30) into (28) and (29), we obtain the following homogeneous system with u, v as unknowns:

$$\begin{pmatrix} \frac{t_a}{\hbar}\cos\left[\left(h + \frac{k}{2}\right)a\right] & -\frac{\Omega_R}{4} \\ -\frac{\Omega_R}{4} & \frac{t_b}{\hbar}\cos\left[\left(h - \frac{k}{2}\right)a\right] \end{pmatrix} \begin{pmatrix} u \\ v \end{pmatrix} = 0. \tag{31}$$

Equation (32) may also be seen from different points of view: Once any two of the three parameters h, k, Ω_R are given, the third one would be considered a required eigenvalue. We assume for simplicity $k = 0$ and find the eigen-wave-number as

$$ha = \pm \arccos\left(\frac{\hbar\Omega_R}{4\sqrt{t_a t_b}}\right). \tag{32}$$

As a result, the steady-state solution (30) becomes

$$|\Psi(t)\rangle = \frac{1}{\sqrt{N}\sqrt{1 + \frac{t_b}{t_a}}} \times \sum_j \left\{ \sqrt{\frac{t_b}{t_a}} e^{-i\frac{\delta\varepsilon}{\hbar}t} |a,j\rangle + e^{i\frac{\delta\varepsilon}{\hbar}t} |b,j\rangle \right\} e^{ihja}. \tag{33}$$

This state exists within the finite range of the ac field values satisfying the inequality $\hbar|\Omega_R| \leqslant 4\sqrt{t_a t_b}$. It may be considered as an analog of the inversion trapped state in a three-level atom Λ configuration [58]. This analogy is incomplete, though, because the inversion trapping in our case is not perfect. The reason for this is in the nonvanishing probability amplitude for the excited state $|a,j\rangle$. However, this value may be made arbitrarily small by making the right choice of the relation between tunneling frequencies, i.e., $t_b \ll t_a$. Thus, in contrast with a three-level atom, the chain of two-level atoms in the state (33) is not perfectly transparent to the incident field, but the reachable values of the photon absorption are arbitrary small if the tunneling in the ground state is suppressed enough as compared with the excited one.

Let us now analyze a wave-packet analog of the coherent trapped state (33). This is done based on the RWA-free Eqs. (19) and (20), and solved numerically with the initial conditions

$$\begin{pmatrix} a_j(0) \\ b_j(0) \end{pmatrix} = g \begin{pmatrix} \sqrt{t_b/t_a} \\ 1 \end{pmatrix} e^{-\frac{(j-j')^2 a^2}{\sigma^2}} e^{ihja} \tag{34}$$

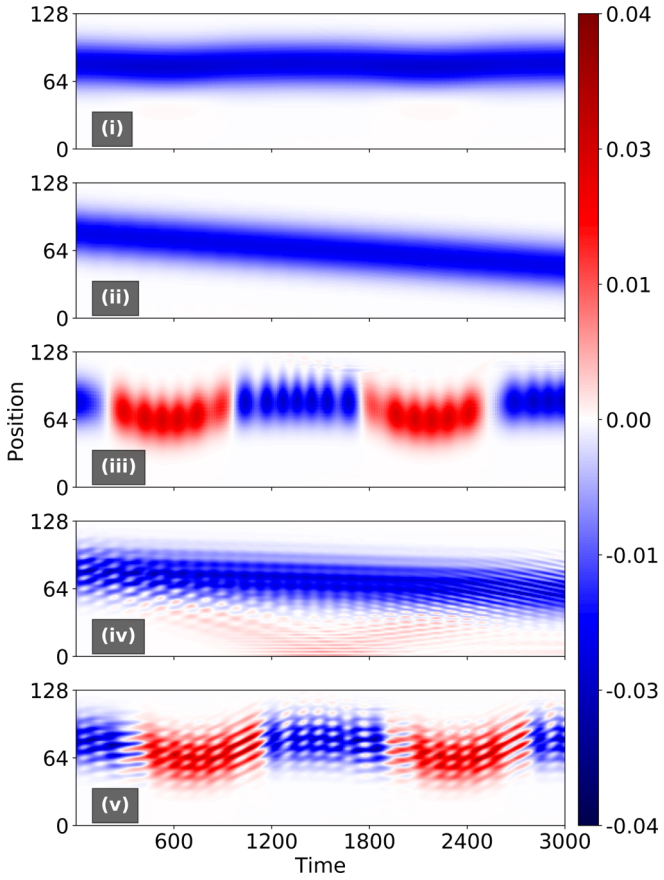

FIG. 12. Space-time distribution of inversion density for the initial state in the form of the Gaussian analog of the inversion trapped state given by Eq. (34). Here, the quantum transition frequency is taken as the frequency unit. Gaussian initial position and width are $p' = 80$, $g = 20$, respectively, Here, interatomic distance $a = 20\,\text{nm}$, $t_a = 3.5 \times 10^{-2}$ eV, $t_b = 3.5 \times 10^{-3}$ eV, and number of atoms is 128. (i) BO case: $\Omega_B = 3.9 \times 10^{-3}$, $\Omega_R = 0$. No BOs have been observed, because of their small amplitude due to the weak tunneling penetration over the barrier for the ground state; (ii) RO case: $\Omega_B = 0$, $\Omega_R = 2.5 \times 10^{-2}$, standing wave ($k = 0$). No ROs have been observed, because of the special interference mechanism of inversion trapping. Progressive motion of the wave packet is dictated by the nonzero value of its initial momentum. (iii) RBO case: $\Omega_B = 3.9 \times 10^{-3}$, $\Omega_R = 2.5 \times 10^{-2}$, standing wave ($k = 0$). Both RO and BO are observed and progressive motion is suppressed due to the combined action of ac and dc fields; (iv) RO case: $\Omega_R = 2.5 \times 10^{-2}$, $\Omega_B = 0$, traveling wave ($ka = -0.624$). No ROs have been observed, similar to case (ii). Progressive motion of the wave packet is accompanied by the spatial beatings dictated by diffraction on the lattice induced by the traveling wave; (v) RBO case: $\Omega_B = 3.9 \times 10^{-3}$, $\Omega_R = 2.5 \times 10^{-2}$, traveling wave ($ka = -0.624$). Both RO and BO are observed similar to case (iii), and accompanied by the spatial beatings similar to case (iv); Case (v): the simultaneous action of both dc and ac fields with $k \neq 0$.

for different relations between the system parameters in the presence of the dc field with g being a normalizing coefficient. Numerical results are shown at Fig. 12. Case (i) corresponds to the ordinary BO. No real oscillations are observed in this case because of their weak amplitude which results from the small value of the tunnel penetration t_b. Case (ii) pertains

to the RO. Here, no oscillations are observed because of the initial-state trapping. The monotonic movement is stipulated by the nonzero initial momentum of the wave packet h. Case (iii) corresponds to RBO (recall that this involves simultaneous action of both dc and ac fields). One can observe Rabi-like oscillations between the ground and excited states. In contrast with the ordinary RO scenario, their frequency is equal to the Bloch frequency and is defined by the value of the dc field. BOs are clearly visible, too, due to tunneling through the exited level with high penetration value, in spite of the small contribution of this state to the total wave function. Case (iv) stands for the Rabi wave, where the picture has changed dramatically due to the trapping of the initial state. The trapped state exhibits spatial oscillations of the wave function that are due to diffraction by the grating and are induced via the field traveling along the array axis ($k \neq 0$), that propagates without interlevel transitions. Case (v) demonstrates both diffraction and interlevel transitions with the Bloch frequency being the result of the simultaneous action of both dc and ac fields with $k \neq 0$. In conclusion, it is found that the dc field in the two-level atomic chain is able to break down the coherence of the trapped states. As a result, the ground and excited states become coupled, which leads to the interlevel oscillations accompanied by BO. This physical mechanism holds promise for a number of potential applications in nanoelectronics, such as electrically controlled nanoantennas and networks.

VI. SUMMARY AND OUTLOOK

By way of summary and open questions, control of the RO is a problem of long-standing interest. As seen above, it is a platform for rich physics, and not in vain, the following question was raised in Ref. [65]: "What can Rabi oscillations teach us?" The same question may be addressed for the BO. This question may be answered in due course when the synthesis of RBO unveils new and exciting capabilities. We hope that this paper has provided the initial steps towards this goal.

In conclusion, we have developed a model of RBO driven by the superposition of dc and ac fields in a one-dimensional chain of two-level atoms coupled via tunneling. We have presented a derivation of the equations of motion for the dc field, which is homogeneous along the chain, and the plane-wave ac field obliquely incident with an arbitrary direction. These equations enable a strong atom-field coupling modeling based on the Wannier basis. Examples of their solutions have been obtained by purely numerical means, demonstrating the spatial-temporal densities of inversion, with dipole current and tunnel current calculated for the system, initiated with a Gaussian packet state.

As a central result, we have shown that the system dynamics is characterized by a superposition of the oscillating interatomic intraband transitions via electron tunneling (BO) and the intra-atomic interband quantum transitions (RO). In spite of such components belonging to different frequency ranges, the RBO dynamics is characterized by strong mutual interaction of Bloch and Rabi components, which qualitatively changes the physical picture of both of them. In particular, we have seen that inversion exhibits the collapse-revival behavior in the inversion in the classical ac field. In this case, the BO propagation plays the role of the photonic dress in the Jaynes-Cummings model [58].

Identifying qualitative behavior of this nature makes the validity of such conventional approximation as RWA a subject of scrutiny. In this regard, we used a model that is free of RWA; however, calculations using the assumption of the RWA have been done, too, and compared with the exact numerical solution. As a result, the RWA was overall shown to reproduce the numerical results qualitatively to a fairly high degree of accuracy through both the approximate solution and a direct numerical implementation of the theory.

Although we have focused on the spectral properties of RBO, the mutual influence of RO and BO interactions was considered in detail. It was shown that the RBO spectrum consists of a low-frequency component (THz) governed by the tunneling, and a high-frequency (optical) component dictated by the interlevel transitions. The complicated behavior of spatial-temporal dynamics leads to the appearance of many additional spectral lines whose amplitudes are compared with the main one.

This opens the door for exciting possibilities of applications in a new type of spectroscopy in nanoelectronics and electrical control in nanodevices. Since the early days of physics, spectroscopy has been a platform for many fundamental, theoretical, and experimental investigations. The first period in the history of spectroscopy is associated with atomic and molecular spectroscopy. Atoms of different elements have distinct spectra, and therefore atomic spectroscopy allows for the identification of a sample's elemental composition. The combination of atoms into molecules leads to the creation of unique types of energetic states and therefore unique spectra of the transitions between these states. The second period in the making of spectroscopy is associated with a wide range of applications for different types of chemical substances, e.g., gases, liquids, crystals, and polymers. The combination of atoms or molecules into macroscopic samples or other extended forms leads to the creation of additional energetic states. Different materials have distinct spectra. Therefore, spectroscopy observations became an irreplaceable tool for the identification of a sample's structure, chemical composition, sample quality, etc., in biophysics, chemistry, and material engineering. Recent progress in nanotechnologies is associated with the synthesis of different types of nano-objects. The distinct spectra became the attribute of nano-objects of different spatial configuration, but with the same chemical composition. In this context, one can envision the future period in the spectroscopy development as being associated with the spectroscopy of the whole range of electronic devices or their rather large components. This trend will provide tools of the tunable spectroscopy adapted for such types of tasks, and the RBO- spectroscopy discussed above may be considered as one of the promising examples from this point of view.

One more subject for future outlook is the manifestation of the quantum origin of light in RBO, in particular, the spontaneous emission of the Rabi-Bloch oscillator. The theory of Bloch dynamics for electrons interacting with vacuum photonic fluctuations in the weak coupling regime was developed in [66]. Such interaction is responsible for spontaneous emission of the Bloch electron, which occurs only with frequencies $\omega = n\Omega_B$, where n is an integer number. The

power emitted spontaneously by the Bloch electron into free space is discernibly small [66]. We expect that the mutual influence of RO and BO will dramatically change the scenario of spontaneous emission considered in [66]. The reason for it is the dressing of Bloch electrons by virtual photons and excitation of vacuum RBO. As a result, the spontaneous emission will be sharply peaked also at frequencies $\omega = \omega_0 + n\Omega_B + m\Omega_R$, where n is an integer number, $m = 0, \pm 1$. Intensities of such lines will be strongly enhanced compared with the weak coupling case. Another problem of interest is the spontaneous emission of coherently trapped RBO considered above. Because of their weak coupling with light, it is reasonable to expect the enhancement of radiative lifetime for such type of excitations. The theoretical framework for the analysis of all these effects is the theory of open quantum systems and master equations technique [58]; this is a subject of a future investigation.

ACKNOWLEDGMENT

G.S. acknowledges support from Project No. FP7-PEOPLE-2013-IRSES-612285 CANTOR.

APPENDIX: DERIVATION OF FORMULA FOR TUNNELING CURRENT

For calculating the tunneling current we introduce the operator of the particle number in the jth atom $\hat{N}_j = |a_j\rangle\langle a_j| + |b_j\rangle\langle b_j|$ and formulate the equation of continuity,

$$\hat{J}_j - \hat{J}_{j-1} = -e\frac{d\hat{N}_j}{dt}, \tag{A1}$$

where $\hat{J}_j$ is the current density operator in the jth atom and the left-hand part in (A1) is a discrete analog of Div in the 1D case. Using the Heisenberg equation for the operator $\hat{N}_j$, we rewrite (A1) in the form

$$\hat{J}_j - \hat{J}_{j-1} = -i\frac{e}{\hbar}[\hat{H}, \hat{N}_j]. \tag{A2}$$

The tunneling currents over excited and background energy levels are independent, thus $\hat{J}_{\text{Tunneling},j} = \hat{J}^{(a)}_{\text{Tunneling},j} + \hat{J}^{(b)}_{\text{Tunneling},j}$. Using (A2), we obtain

$$\hat{J}^{(a,b)}_{\text{Tunneling},j} - \hat{J}^{(a,b)}_{\text{Tunneling},j-1} = -i\frac{e}{\hbar}\left[\hat{H}^{(a,b)}_{\text{Tunneling}}, \hat{N}_j\right], \tag{A3}$$

where

$$\hat{H}^{(a)}_{\text{Tunneling}} = \sum_j \left(t_a|a,j\rangle\langle a,j+1| + t_a^*|a,j\rangle\langle a,j-1|\right) \tag{A4}$$

is a component of thee Hamiltonian (10), chargeable for the tunneling at the excited level (a similar equation may be written for the Hamiltonian $\hat{H}^{(b)}_{\text{Tunneling}}$). Using (A4), we calculate the commutator in the right-hand part of (A3) and obtain

$$\hat{J}^{(a)}_{\text{Tunneling},j} - \hat{J}^{(a)}_{\text{Tunneling},j-1} = -iet_a(|a_{j-1}\rangle + |a_{j+1}\rangle)\langle a_j| + \text{H.c.} \tag{A5}$$

It corresponds to the operator of the tunneling current at the excited level

$$\hat{J}^{(a)}_{\text{Tunneling},j} = -iet_a|a_j\rangle\langle a_{j+1}| + \text{H.c.} \tag{A6}$$

The observable value of the tunneling current is

$$J^{(a)}_{\text{Tunneling},j}(t) = \left\langle \hat{J}^{(a)}_{\text{Tunneling},j} \right\rangle = -iet_a a_j^*(t)a_{j-1}(t) + \text{c.c.} \tag{A7}$$

Using the approximation $a_{j-1}(t) - a_j(t) \approx [a_{j+1}(t) - a_{j-1}(t)]/2$, and adding the similar support of the ground level, we obtain the relation (24). This relation corresponds to the well-known definition of the probability flow $\mathbf{j} = i\hbar(\Psi \text{grad}\Psi^* - \text{c.c.})/2m$ in the 3D continuous case [61].

[1] E. Ising, Beitrag zur Theorie des Ferromagnetismus, Z. Phys. **31**, 253 (1925).

[2] W. Heisenberg, Zur Theorie der Ferromagnetismus, Z. Phys. **49**, 619 (1928).

[3] J. Hubbard, Electron correlations in narrow energy bands, Proc. R. Soc. London **276**, 1365 (1963).

[4] L. Esaki and R. Tsu, Superlattice and negative differential conductivity in semiconductors, IBM J. Res. Dev. **14**, 61 (1970).

[5] R. V. Gorbachev, J. S. W. Song, G. L. Yu, A. V. Kretinin, F. Withers, Y. Cao, A. Mishchenko, I. V. Grigorieva, K. S. Novoselov, L. S. Levitov, and A. K. Geim, Detecting topological currents in graphene superlattices, Science **346**, 6208 (2014).

[6] G. Dong, J. Zhu, W. Zhang, and B. A. Malomed, Polaritonic Solitons in a Bose-Einstein Condensate Trapped in a Soft Optical Lattice, Phys. Rev. Lett. **110**, 250401 (2013).

[7] P. Hauke, D. Marcos, M. Dalmonte, and P. Zoller, Quantum Simulation of a Lattice Schwinger Model in a Chain of Trapped Ions, Phys. Rev. X **3**, 041018 (2013).

[8] S. Braungardt, A. S. De, U. Sen, and M. Lewenstein, Error-resistant distributed quantum computation in a trapped ion chain, Phys. Rev. A **76**, 042307 (2007).

[9] O. S. Mishina, Cavity cooling of an atomic array, New J. Phys. **16**, 033021 (2014).

[10] F. Maibaum, S. V. Lotkhov, and A. B. Zorin, Towards the observation of phase-locked Bloch oscillations in arrays of small Josephson junctions, Phys. Rev. B **84**, 174514 (2011).

[11] D. Heitmann and J. R. P. Kotthaus, The spectroscopy of quantum dot arrays, Phys. Today **46**(6), 56 (1993).

[12] G. Ya. Slepyan, S. A. Maksimenko, V. P. Kalosha, A. Hoffmann, and D. Bimberg, Effective boundary conditions for planar quantum dot structures, Phys. Rev. B **64**, 125326 (2001).

[13] G. Ya. Slepyan and S. A. Maksimenko, Photon-statistics dispersion in excitonic composites, New J. Phys. **10**, 023032 (2008).

[14] J. Cai and G. D. Mahan, Energy bands of quantum dot arrays, Phys. Rev. B **76**, 205116 (2007).

[15] J. Cai and G. D. Mahan, Transport properties of quantum dot arrays, Phys. Rev. B **78**, 035115 (2008).

[16] G. Weiser, L. Legrand, T. Barisien, A. Al Choueiry, M. Schott, and S. Dutremez, Stark effect and Franz-Keldysh effect of a quantum wire realized by conjugated polymer chains of a diacetylene 3NPh2, Phys. Rev. B **81**, 125209 (2010).

[17] A. Yu. Kitaev, Unpaired Majorana fermions in quantum wires, Phys.-Usp. **44**, 131 (2001).
[18] M. A. Nielsen and I. L. Chuang, *Quantum Computation and Quantum Information* (Cambridge University Press, Cambridge, UK, 2000).
[19] D. Mogilevtsev, G. Ya. Slepyan, E. Garusov, S. Ya. Kilin, and N. Korolkova, Quantum tight-binding chains with dissipative coupling, New J. Phys. **17**, 043065 (2015).
[20] D. Mogilevtsev and G. Ya. Slepyan, Diffusive lossless energy and coherence transfer by noisy coupling, Phys. Rev. A **94**, 012116 (2016).
[21] S. Mukherjee, D. Mogilevtsev, G. Ya. Slepyan, Th. H. Doherty, R. R. Thomson, and N. Korolkova, Coherent diffusive photonics, arXiv:1703.06025.
[22] D.-W. Wang, R.-B. Liu, S.-Y. Zhu, and M. O. Scully, Superradiance Lattice, Phys. Rev. Lett. **114**, 043602 (2015).
[23] G. Ya. Slepyan, Y. D. Yerchak, S. A. Maksimenko, and A. Hoffmann, Wave propagation of Rabi oscillations in one-dimensional quantum dot chain, Phys. Lett. A **373**, 1374 (2009).
[24] G. Ya. Slepyan, Y. D. Yerchak, S. A. Maksimenko, A. Hoffmann, and F. G. Bass, Mixed states in Rabi waves and quantum nanoantennas, Phys. Rev. B **85**, 245134 (2012).
[25] Y. Yerchak, G. Y. Slepyan, S. A. Maksimenko, A. Hoffmann, and F. Bass, Array of tunneling-coupled quantum dots as a terahertz range quantum nanoantenna, J. Nanophotonics **7**, 073085 (2013).
[26] G. Ya. Slepyan, Y. D. Yerchak, A. Hoffmann, and F. G. Bass, Strong electron-photon coupling in a one-dimensional quantum dot chain: Rabi waves and Rabi wave packets, Phys. Rev. B **81**, 085115 (2010).
[27] G. Gligorić, A. Maluckov, L. Hadzievski, G. Ya. Slepyan, and B. A. Malomed, Discrete solitons in an array of quantum dots, Phys. Rev. B **88**, 155329 (2013).
[28] G. Gligorić, A. Maluckov, L. Hadzievski, G. Ya. Slepyan, and B. A. Malomed, Soliton nanoantennas in two-dimensional arrays of quantum dots, J. Phys.: Condens. Matter **27**, 225301 (2015).
[29] Y. Hadad, Y. Mazor, and B. Z. Steinberg, Green's function theory for one-way particle chains, Phys. Rev. B **87**, 035130 (2013).
[30] G. Y. Slepyan and A. Boag, Quantum Nonreciprocity of Nanoscale Antenna Arrays in Timed Dicke States, Phys. Rev. Lett. **111**, 023602 (2013).
[31] F. Bloch, Über die Quantenmechanik der Elektronen in Kristallgittern, Z. Phys. **52**, 555 (1929).
[32] C. Zener, A theory of electrical breakdown of solid dielectrics, Proc. R. Soc. London, Ser. A **145**, 523 (1934).
[33] G. H. Wannier, Wave functions and effective Hamiltonian for Bloch electrons in an electric field, Phys. Rev. **117**, 432 (1960).
[34] G. H. Wannier, Stark ladder in solids? A reply, Phys. Rev. **181**, 1364 (1969).
[35] M. Gluck, A. R. Kolovsky, and H. J. Korsch, Wannier–Stark resonances in optical and semiconductor superlattices, Phys. Rep. **366**, 103 (2002).
[36] T. Hartmann, F. Keck, H. J. Korsch, and S. Mossmann, Dynamics of Bloch oscillations, New J. Phys. **6**, 2 (2004).
[37] J. Feldmann, K. Leo, J. Shah, D. A. B. Miller, J. E. Cunningham, T. Meier, G. von Plessen, A. Schulze, P. Thomas, and S. Schmitt-Rink, Optical investigation of Bloch oscillations in a semiconductor superlattice, Phys. Rev. B **46**, 7252(R) (1992).
[38] K. Leo, P. H. Bolivar, F. Brüggemann, and R. Schwedler, Observation of Bloch oscillations in a semiconductor superlattice, Solid State Commun. **84**, 943 (1992).
[39] M. Ben Dahan, E. Peik, J. Reichel, Y. Castin, and C. Salomon, Bloch Oscillations of Atoms in an Optical Potential, Phys. Rev. Lett. **76**, 4508 (1996).
[40] S. Wilkinson, C. Bharucha, K. Madison, Q. Niu, and M. Raizen, Observation of Atomic Wannier-Stark Ladders in an Accelerating Optical Potential, Phys. Rev. Lett. **76**, 4512 (1996).
[41] R. Morandotti, U. Peschel, J. S. Aitchison, H. S. Eisenberg, and Y. Silberberg, Experimental Observation of Linear and Nonlinear Optical Bloch Oscillations, Phys. Rev. Lett. **83**, 4756 (1999).
[42] T. Pertsch, P. Dannberg, W. Elflein, A. Bräuer, and F. Lederer, Optical Bloch Oscillations in Temperature Tuned Waveguide Arrays, Phys. Rev. Lett. **83**, 4752 (1999).
[43] U. Peschel, T. Pertsch, and F. Lederer, Optical Bloch oscillations in waveguide arrays, Opt. Lett. **23**, 1701 (1998).
[44] M. J. Zheng, J. J. Xiao, and K. W. Yu, Controllable optical Bloch oscillation in planar graded optical waveguide arrays, Phys. Rev. A **81**, 033829 (2010).
[45] Y. Bromberg, Y. Lahini, and Y. Silberberg, Bloch Oscillations of Path-Entangle Photons, Phys. Rev. Lett **105**, 263604 (2010); **106**, 149902(E) (2011).
[46] I. Afek, A. Natan, O. Ambar, and Y. Silberberg, Quantum state measurements using multipixel photon detectors, Phys. Rev. A **79**, 043830 (2009).
[47] I. Afek, O. Ambar, and Y. Silberberg, High-N00N states by mixing quantum and classical light, Science **328**, 879 (2010).
[48] M. Lebugle, M. Gräfe, R. Heilmann, A. Perez-Leija, S. Nolte, and A. Szameit, Experimental observation of N00N state Bloch oscillations, Nat. Commun. **6**, 8273 (2015).
[49] K. Kudo and T. S. Monteiro, Theoretical analysis of super–Bloch oscillations, Phys. Rev. A **83**, 053627 (2011).
[50] H. Lignier, C. Sias, D. Ciampini, Y. Singh, A. Zenesini, O. Morsch, and E. Arimondo, Dynamical Control of Matter-Wave Tunneling in Periodic Potentials, Phys. Rev. Lett. **99**, 220403 (2007).
[51] C. Sias, H. Lignier, Y. P. Singh, A. Zenesini, D. Ciampini, O. Morsch, and E. Arimondo, Observation of Photon-Assisted Tunneling in Optical Lattices, Phys. Rev. Lett. **100**, 040404 (2008).
[52] E. Kierig, U. Schnorrberger, A. Schietinger, J. Tomkovic, and M. K. Oberthaler, Single-Particle Tunneling in Strongly Driven Double-Well Potentials, Phys. Rev. Lett. **100**, 190405 (2008).
[53] A. Eckardt, M. Holthaus, H. Lignier, A. Zenesini, D. Ciampini, O. Morsch, and E. Arimondo, Exploring dynamic localization with a Bose-Einstein condensate, Phys. Rev. A **79**, 013611 (2009).
[54] A. Alberti, V. V. Ivanov, G. M. Tino, and G. Ferrari, Engineering the quantum transport of atomic wavefunctions over macroscopic distances, Nat. Phys. **5**, 547 (2009).
[55] E. Haller, R. Hart, M. J. Mark, J. G. Danzl, L. Reichsollner, and H. C. Nagerl, Inducing Transport in a Dissipation-Free Lattice with Super Bloch Oscillations, Phys. Rev. Lett. **104**, 200403 (2010).
[56] A. Zenesini, H. Lignier, D. Ciampini, O. Morsch, and E. Arimondo, Coherent Control of Dressed Matter Waves, Phys. Rev. Lett. **102**, 100403 (2009).

[57] X.-G. Zhao, G. A. Georgakis, and Q. Niu, Rabi oscillations between Bloch bands, Phys. Rev. B **54**, R5235(R) (1996).
[58] M. O. Scully and M. Zubairy, *Quantum Optics* (Cambridge University Press, Cambridge, 2001).
[59] P. P. Yu and M. Cardona, *Fundamentals of Semiconductors: Physics and Material Properties* (Springer, Berlin, 2001).
[60] T. F. Gallagher, *Rydberg Atoms* (Cambridge University Press, Cambridge, 1994).
[61] L. D. Landau, and E. M. Lifshitz, *Quantum Mechanics, Course of Theoretical Physics* (Pergamon Press, Oxford, 1965).
[62] O. V. Kibis, G. Ya. Slepyan, S. A. Maksimenko, and A. Hoffmann, Matter Coupling to Strong Electromagnetic Fields in Two-Level Quantum Systems with Broken Inversion Symmetry, Phys. Rev. Lett. **102**, 023601 (2009).
[63] A. A. Svidzinsky, J.-T. Chang, and M. O. Scully, Cooperative spontaneous emission of N atoms: Many-body eigenstates, the effect of virtual Lamb shift processes, and analogy with radiation of N classical oscillators, Phys. Rev. A **81**, 053821 (2010).
[64] U. Peskin and M. Galperin, Coherently controlled molecular junctions, J. Chem. Phys. **136**, 044107 (2012).
[65] J. I. Fuks, N. Helbig, I. V. Tokatly, and A. Rubio, Nonlinear phenomena in time-dependent density-functional theory: What Rabi oscillations can teach us, Phys. Rev. B **84**, 075107 (2011).
[66] V. N. Sokolov, L. Zhou, G. J. Iafrate, and J. B. Krieger, Spontaneous emission of Bloch oscillation radiation from a single energy band, Phys. Rev. B **73**, 205304 (2006).